# Nanoindentation study of PVD WC/C coatings supported by cross- sectional electron microscopy observations

Carvalho, N.J.M.; de Hosson, J.T.M.

*Published in:*
Surface Engineering

*DOI:*
10.1179/026708401101517674

# Characterization of mechanical properties of tungsten carbide/carbon multilayers: Cross-sectional electron microscopy and nanoindentation observations

N.J.M. Carvalho and J.Th.M. De Hosson[a)]
*Department of Applied Physics, Materials Science Center and Netherlands Institute of Metals Research, University of Groningen, Nijenborgh 4, 9747 AG Groningen, The Netherlands*

(Received 11 January 2001; accepted May 2001)

Multilayers of tungsten carbide/carbon (WC/C) deposited by physical vapor deposition onto steel substrates were subjected to depth-sensing indentation testing. The investigation aimed at probing the influence of dissimilarities between the microstructure of the multilayers and substrate on the system mechanical properties. The resultant load-displacement data were analyzed both by conventional load-displacement ($P$-$\delta$) and load-displacement squared ($P$-$\delta^2$) plots. Furthermore, it was demonstrated that the occurrence of annular through-thickness cracks around the indentation sites can be identified from the load-displacement curve. Also, analysis of the lower part of the unloading curve permitted us to identify whether the coating had popped up by localized fracture. The cracking mechanism was characterized using a new technique for cross-sectional electron microscopy of the nanoindentations. The information retrieved with this technique eliminates the problems, inherent in assessing at this small contact scales, whether the fracture is by coating decohesion or by interfacial failure. In our case, it was demonstrated that the failure mechanism was decohesion of the carbon lamellae within the multilayers. The mechanical properties (hardness and effective Young's modulus) were also assessed by nanoindentation. The hysteresis loops were analyzed and discussed in terms of the method developed by Oliver and Pharr [J. Mater. Res. **7,** 1564 (1992)].

## I. INTRODUCTION

Tungsten carbide/carbon (WC/C) deposited by physical vapor deposition (PVD) has received considerable attention in recent years, owing to its low friction coefficient and high wear resistance[1,2] in combination with substrate temperatures of 200 to 400 °C achieved during deposition. Furthermore, the fact that adhesion between the coating and the substrate has been improved by depositing an interlayer of chromium[3] has helped to promote the deposition of such coatings onto machine components subjected to a high shear stress component. However, if the advantages are to be fully employed in improving the surface properties of engineering components, it is necessary to understand more thoroughly the detailed mechanisms by which surface properties are improved.

Ultralow load indentation (nanoindentation) experiments have become increasingly widespread to gauge the mechanical properties of coated systems. The appeal of this technique is that very low loads and displacements are available, enabling characterization on a submicrometer scale. These features permit mechanical property data to be obtained from thin films not only in the microstructural and residual stress state in which they exist as coatings while on a substrate, but also in a regime where their properties should dominate.[4,5] The combination of load-displacement data obtained from nanoindentation cycle with post mortem observation of the indentations, using either scanning electron microscopy (SEM) or scanning force microscopy, reveals important aspects of the contact-induced fracture of coated systems.[6,7] However, complementary information is needed regarding any delamination at the indentation sites. Techniques such as scanning electron acoustic microscopy[8] and Nomarski interference light microscopy[9] have been used to examine delamination, although the resolutions are found to be too low. To overcome this lack of information, we have developed a method for cross-sectioning the samples through the contact sites, allowing direct measurement of the fracture mechanism. Moreover, the method permits cross-sectional scanning/transmission electron microscopy (SEM/TEM) of the resulting

[a)]Address all correspondence to this author.
e-mail: hossonj@phys.rug.nl

  

nanoindentations. A thorough study of the deposition process, microstructure, and chemical composition of the systems has been described elsewhere.[10] Therefore, in this article information is only given about the structure of the systems whenever it is required to understand their surface deformation behavior. The use of different coatings–substrates configurations reveals important clues with respect to the mechanical behavior of the entire coating system. A thorough assessment of elastic, plastic, and fracture properties of the coated systems was performed by nanoindentation experiments. Advanced electron microscopy techniques were used to retrieve complementary information regarding the delamination mechanisms.

## II. EXPERIMENTAL PROCEDURES

### A. Substrate materials

The coatings examined in this work were deposited onto stainless steel (AISI 304) and tool steel (AISI D2) substrates with a rectangular (90 × 10 × 3 mm) geometry. The tool steel was heat treated and tempered at 520 °C to obtain 60 Hardness-Rockwell (HRC). The surfaces were finished by polishing to an average roughness, $R_a$, of 0.03, 0.05, and 0.07 μm. Then, three dissimilar WC/C coatings, denoted S1, S2, and T1, were deposited onto those substrates in a BAI 830 coating unit by Balzers Ltd., Liechtenstein. The combinations of coating/substrate evaluated in this study are presented in Table I.

TABLE I. Coated systems investigated in this work.

| Sample ID | Substrate material | Substrate hardness *HV* (GPa) | Substrate roughness $R_a$ (μm) | Coating thickness (μm) | Coating roughness $R_a$ (μm) |
|---|---|---|---|---|---|
| S1 | Stainless steel (AISI 304) | 1.6 | 0.05 | 3 | 0.05 |
| S2 | Stainless steel (AISI 304) | 1.6 | 0.03 | 2.8 | 0.05 |
| T1 | Tool steel (AISI D2) | 6.8 | 0.07 | 2.7 | 0.06 |

### B. Hardness and elastic modulus

To determine the hardness and elastic properties of the material from a nanoindentation response several methods have been developed, all being based on contact mechanics.[11–14] The hardness and elastic modulus were calculated from the load-displacement curve using the following equations.

$$H = \frac{P_{\max}}{A} \quad , \tag{1}$$

$$E_r = \frac{\sqrt{\Pi}}{2} \frac{S}{\beta\sqrt{A}} \quad , \tag{2}$$

where $P$ is the maximum applied load, $A$ is the projected area of the elastic contact, $E_r$ is the reduced elastic modulus, β is a geometrical correction factor accounting for the cross-sectional shape of the indenter equal to 1.034, and $S$ is the experimentally measured contact stiffness; e.g., using the procedure of Oliver and Pharr,[14] it corresponds to the slope of the unloading curve during the initial stages of unloading. The reduced modulus, $E_r$, is used in the analysis to account for the fact that the elastic deformation occurs in both the specimen and indenter. It is related to the specimen modulus through

$$\frac{1}{E_r} = \frac{(1-\nu^2)}{E} + \frac{(1-\nu_i^2)}{E_i} \quad , \tag{3}$$

where $E$ and $\nu$ are the Young's modulus and Poisson's ratio for the specimen and $E_i$ and $\nu_i$ are the same quantities for the diamond indenter. When the Poisson's ratio for the specimen is unknown an effective elastic modulus is used instead:

$$E_{\text{eff}} = \frac{E}{1-\nu^2} \quad . \tag{4}$$

Nanoindentation experiments were carried out using a home-made apparatus with a Berkovich diamond tip, which was described elsewhere.[15] Indentation cycles were made under both load and displacement control to peak loads ranging from 10 mN to 1 N. For each load a series of at least ten indentations was made and a mean value for the hardness and effective modulus was determined. The standard deviation was used as a measure of the experimental uncertainty.

### C. Nanoindentation cross-sectioning procedure

To investigate the coated system response beneath the trigonal impression of a nanoindentation, cross-sectional TEM specimens from the contact sites were prepared. The novel method developed is as follows. Two thin slabs (1,300 × 50 × 350 μm) of coated material with the coating on the 1,300 × 50 μm surface were fitted in a 100-μm-wide slot of a titanium grid. Then three rows of indentations, distributed over the coated surface, were performed in each specimen with a load ranging between 50 mN and 400 mN. After performing the indentations, the slabs were removed from the grid and fitted film-to-film in a 700-μm-wide slot and then embedded in a two-component glue. When the glue was cured, which was accomplished by placing the specimen in a temperature-controlled oven, it was polished (using a Tripod Polisher) to remove 10 μm of material from each side. Subsequently, ion-beam milling was performed by using two guns in mirror-image positions on both sides of the rotating specimen using a Gatan PIPS, model 691.

The angle of incidence was 6° (ion energy 4 kV and ion current 40 μA). Final thinning to electron transparency was accomplished by rocking the specimen ±30° perpendicular to the coating–substrate interface with an incoming ion beam at 4°. This process continued until perforation took place and the hole reached the region of interest. Finally, the surface contaminants (due to redeposited material) were reduced by using an ion energy of 2 kV and ion current of 4 μA while continuing rocking the specimen. To ensure that the electron transparent area was in the desired region, the ion milling was periodically stopped and the specimen was examined with SEM. SEM of the indentations was performed using a Philips XL 30-FEG microscope (Eindhoven, The Netherlands), and for higher magnification, TEM was employed using a JEOL 4000 EX/II microscope (Tokyo, Japan). Depth information from the nanoindentations hardness impression was obtained by using a μSurf (Nanofocus) confocal microscope with an Olympus lens (100×/0.95). With this configuration, a 10-nm depth resolution was obtained.

## III. RESULTS AND DISCUSSION

The microstructure of the WC/C coatings is disclosed by overview cross-sectional TEM images in Fig. 1. They are formed by (A) a chromium interlayer, (B) an intermultilayer of WC and carbon, (C) a WC layer, and (D) the WC/C multilayers.

### A. Nanoindentation response

Considerable insight into the behavior of coated systems can be gained from their load-displacement displacement response, especially when a comparison is made with that of the substrate alone. Figure 2 shows the load-displacement responses of the two substrate materials for two independent indentations. The responses are typical of ductile materials. The loading curves are parabolic and the unloading segment displays little elastic recovery of the indentation depth. Plastic deformation is evident even at lower loads, being more pronounced on the 304 stainless steel due to its higher ductility.

The load-displacement curves for the coated systems are shown in Fig. 3. The response when compared to the substrate material demonstrates that the load-displacement curve for low peak loads exhibits an increased amount of elastic recovery on unloading, establishing that a higher proportion of the deformation is accommodated elastically. This is observed by smaller displacements at maximum load, and reductions in the elastic and plastic works of indentation. Thus, the influence of the substrate is much reduced, evidencing that at these contact loads the response of the system is mainly characterized by the coating properties. At higher peak loads, however, corresponding to an indentation depth considerably less than the coating thickness, the elastic recovery is more related to the substrate, indicating that the relative contribution of the coating to the system has been reduced.

The load-displacement curves displayed in Fig. 3 from WC/C onto stainless steel exhibits a discrete change in the slope of the loading curve at approximately 150 mN for system S1 and at approximately 120 mN for system S2. However, the WC/C films deposited onto tool steel do not exhibit such a change. SEM micrographs from systems S1 and S2 showed that indentations whose peak

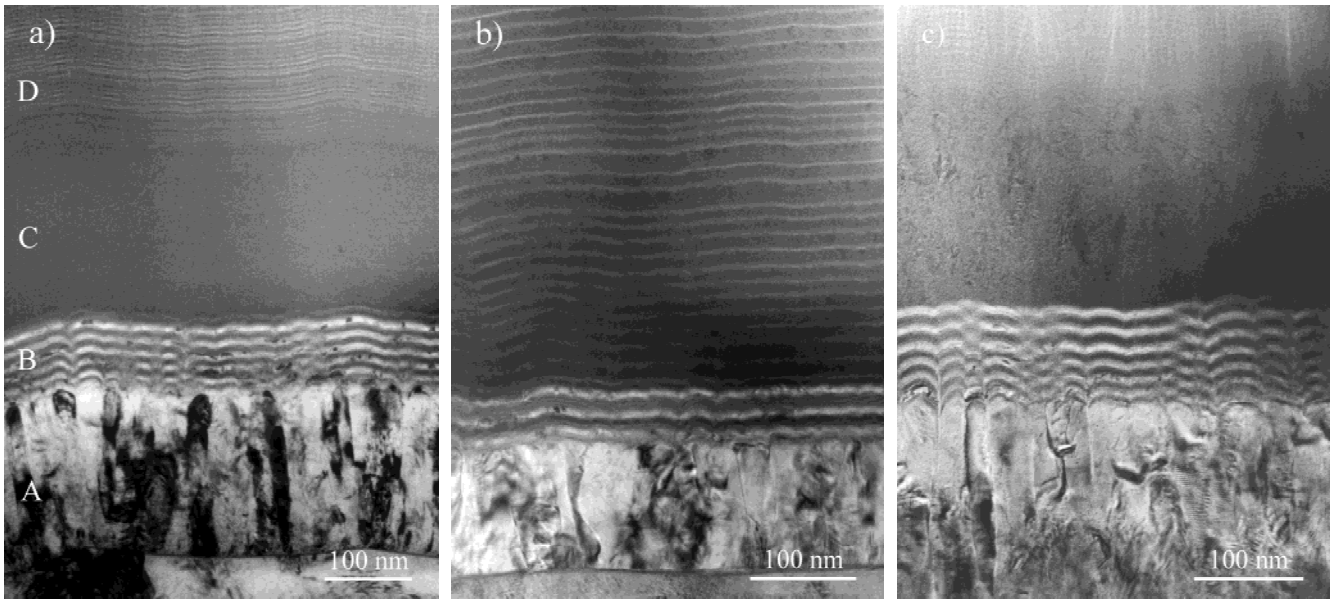


FIG. 1. Cross-sectional TEM micrographs showing the microstructure of the coatings investigated in this study: (a) system S1, (b) system S2, (c) system T1. The structure of the coatings consisted of a chromium interlayer (A), an intermultilayer (B), a WC layer (C) for systems S1 and T1, and the WC/C multilayers (D).

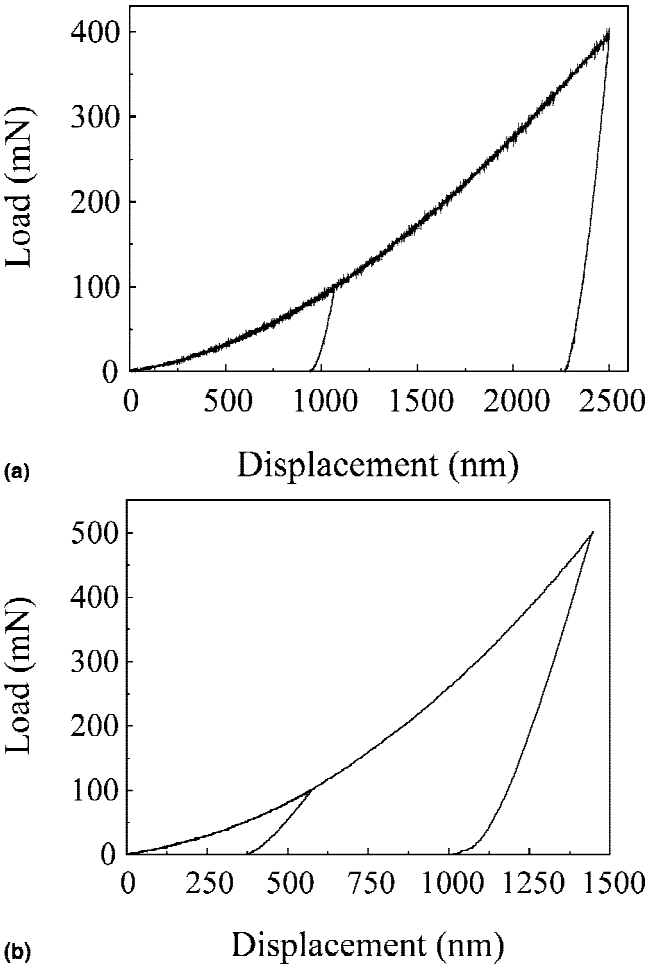


FIG. 2. Nanoindentation load-displacement curves of the steel substrates: (a) indentations with peak loads of 100 and 400 mN on stainless steel, and (b) indentations with peak loads of 100 and 500 mN on tool steel. The responses are typical of plasticity dominated materials, showing a parabolic loading curve and an unloading segment more or less vertical.

load is lower than the value of decrease in slope reveal no signs of coating failure, whereas for higher loads the indentation had always an annular crack around the periphery. The fact that the initial unloading contact stiffness from the load-displacement curve of Fig. 3(b) is not dominated by the modulus of the substrate only [cf. Fig. 2(a)], indicates that the annular crack is not a complete through thickness. Increasing the peak load, there is an additional flexing of the coating around the periphery of the impression and formation of more annular cracks. Then, the initial unloading contact stiffness approximates the one controlled by the modulus of the substrate. At approximately 700 mN the unloading is controlled only by the substrate modulus. In this situation it is believed that the first annular crack has developed completely through thickness.

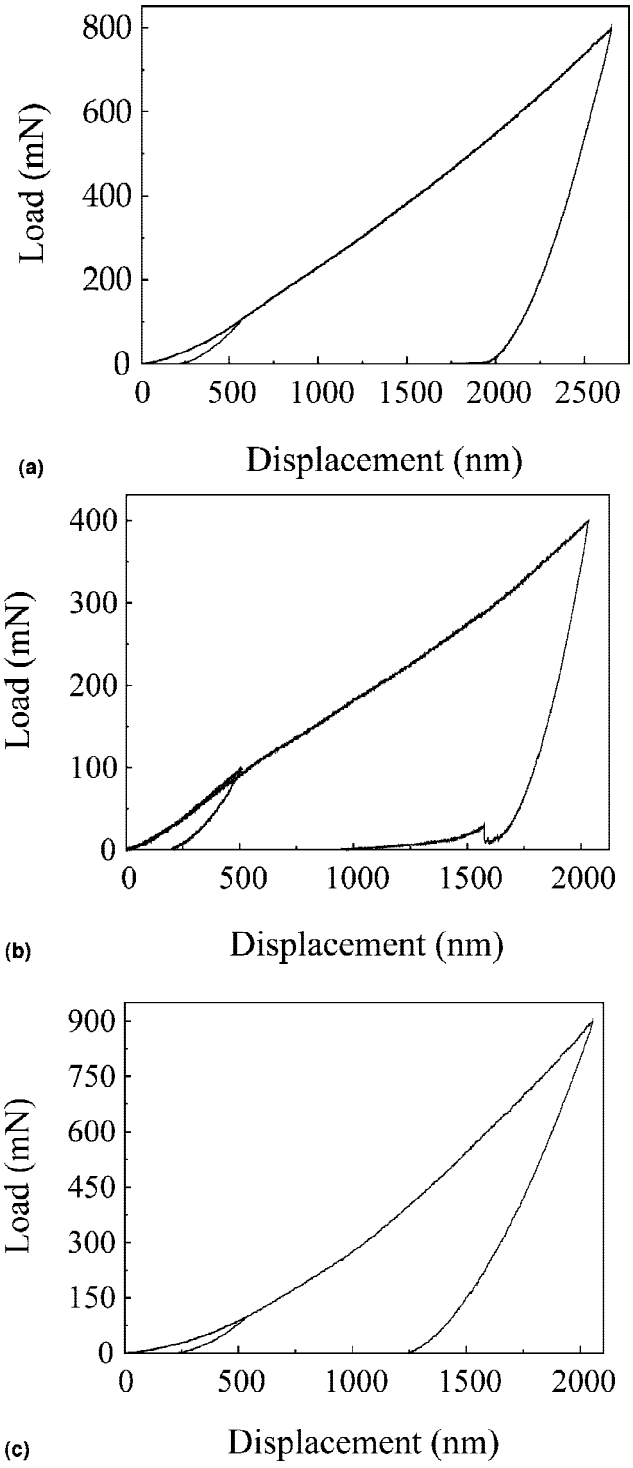


FIG. 3. Nanoindentation load-displacement curves of the three coated system: (a) Response of system S1 to peak loads higher and lower than the decrease in slope, which takes place at approximately 150 mN (best seen at a glancing angle). (b) Response of system S2 for the same situation as described above, although in this case the change in slope occurs at approximately 120 mN. The last stages of unloading show the uplifting of the coating. (c) Response of system T1 for indentations at two different peak loads showing no decrease in slope. Note the different values of peak loads that had to be used to achieve an equivalent maximum total surface deflection.

The nanoindentation response from coating system T1 did not show any change in slope for the load range employed in this study (10 mN up to 1 N). Instead, the SEM micrographs from higher peak load indentations showed the presence of nested cracks following the indentation profile. Thus, the crack pattern is more related to the substrate deformation mechanism, rather than the one of the coating. Figure 4 presents SEM micrographs of nanoindentation response of the coated systems. The micrographs were taken from the indentation impression at the higher loads of Fig. 3. The existence of annular cracks in the case of stainless steel substrate suggests that significant tensile stresses were generated around the outer periphery of the contact zone by coating flexure and upthrust of the substrate material (pile-up) due to displacement by plastic flow.[9] Conversely, the nested cracks for tool steel substrate indicate that the coating has been bent and stretched as the substrate yields and plastically deforms to accommodate the indenter displacements.[16]

Hainsworth and Page[17] have proposed that changes in the slope of load-displacement squared ($P$-$\delta^2$) can be used to assess the transition between the different regimes of coated system behavior. In this model, the load-displacement squared curve shows three distinct regions. Initially, the indenter should just probe the properties of the coating, which should be reflected by a straight line. Then, there is a transition region where the properties of the coating and substrate are probed. Subsequently, the curve should again be a straight line reflecting the properties of the substrate alone. Figure 5 shows the $P$-$\delta^2$ data for the indentations on the coated systems (obtained from the $P$-$\delta$ curves of Fig. 3). The $P$-$\delta^2$ graphs of Figs. 5(a) and 5(b) display the three distinct regimes of coated materials. The first regime is characterized by a straight line segment, which is believed to be related to the coating properties. Then there is the transition region, where the properties of both the coating and substrate are revealed. Within this region, the substrate deforms plastically causing the coating to crack around the indentation periphery, originating the annular crack. At large displacements, the fractured coating will play an insignificant role in supporting the applied load. Thus, a second straight line segment emerges, whose slope is approximately controlled by the substrate properties, representing the last regime. The small nonlinear segment at the beginning of the graph is thought to be caused by a combination of tip shape imperfections and any elastic-only deformation of the coating as the tip first makes contact with the surface.[18]

The $P$-$\delta^2$ graph displayed in Fig. 5(c) for coating system T1, does not clearly reveal the transition between the coating and substrate domination of the indentation response. Therefore, when the coating fracture is via nested cracks instead of annular cracks, the membrane stresses

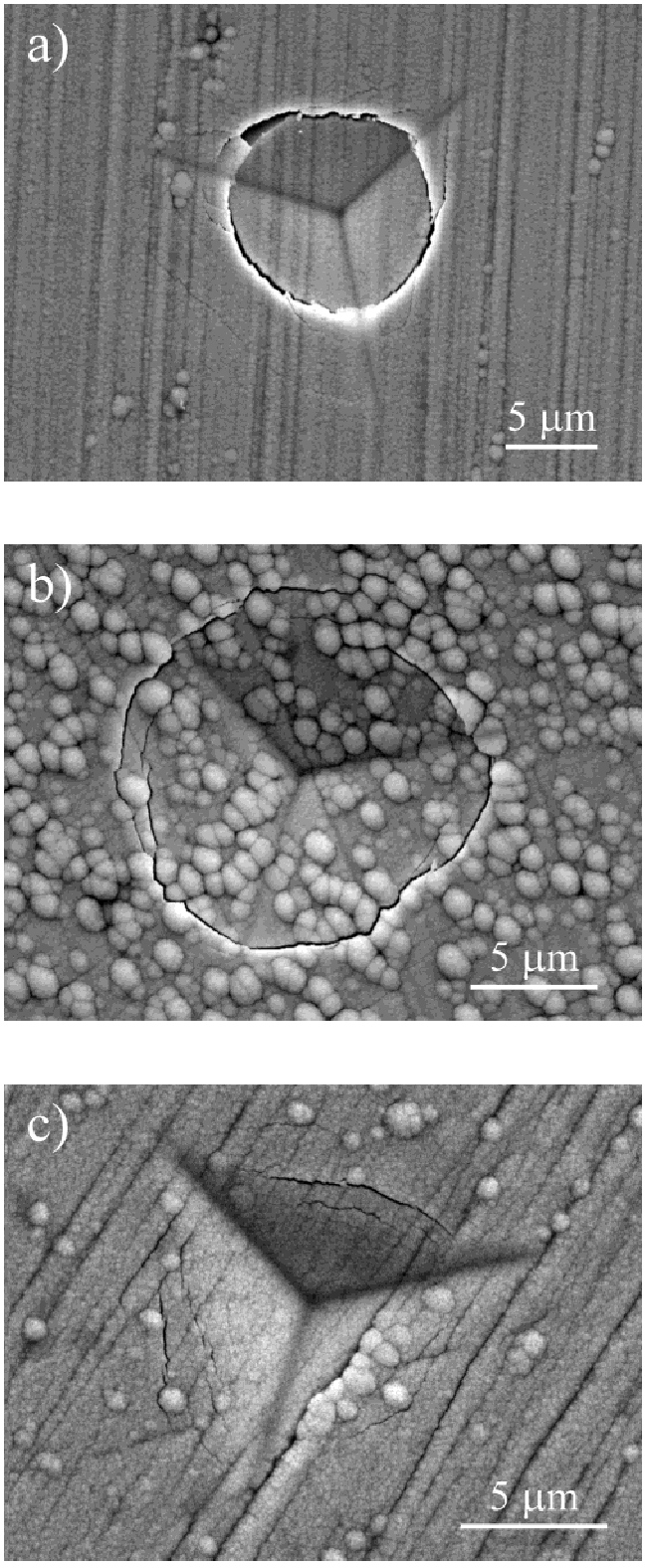


FIG. 4. SEM micrographs showing the indentations impression on coated systems: (a) 800-mN nanoindentation on system S1, (b) 400-mN nanoindentation on system S2, and (c) 900-mN nanoindentation on system T1. The first two display annular cracks, whereas the latter fractures through nested cracks.

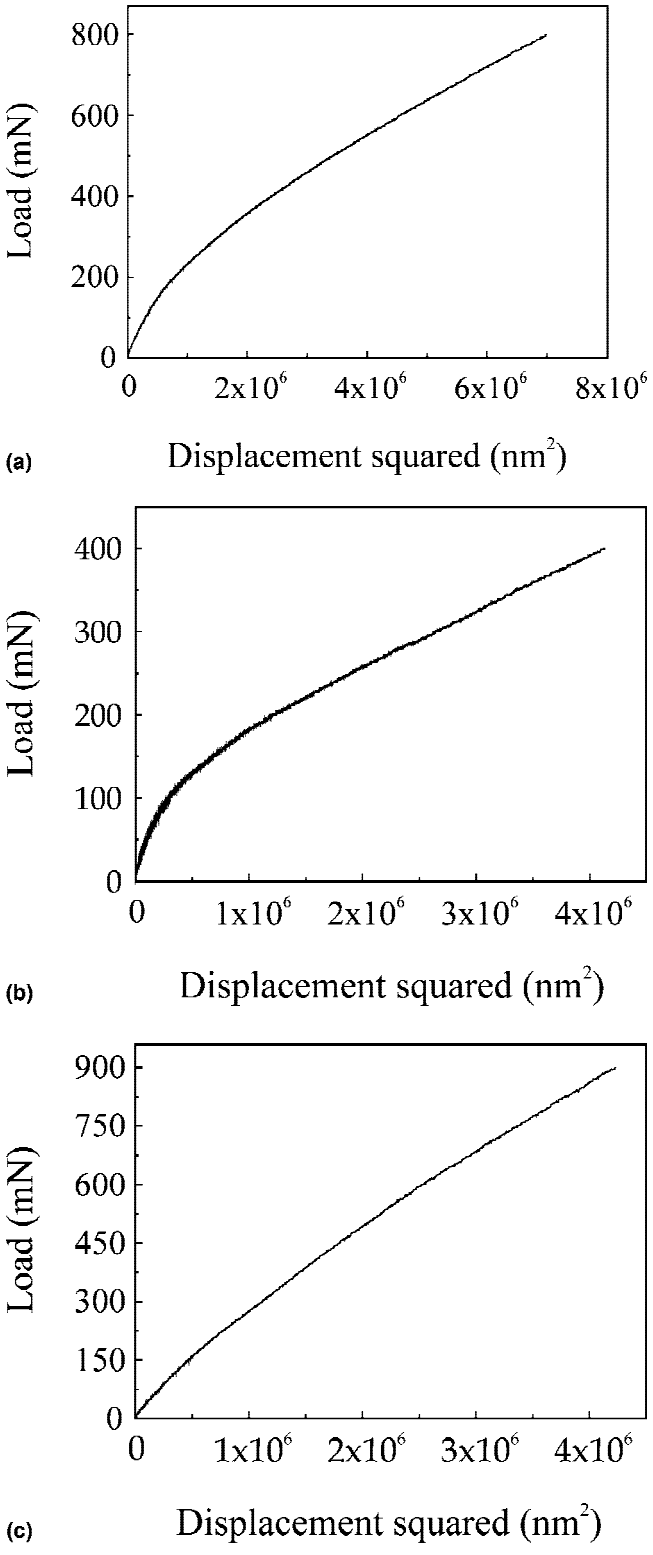


FIG. 5. Load-displacement data corresponding to the higher peak loads of Fig. 3 replotted as load-displacement squared. Curves (a) and (b) are of systems S1 and S2, respectively. As these systems have a stainless steel substrate, the transition between the differing regimes of behavior is undoubtedly observed (see text). Curve (c) of system T1 does not display so clearly the change of coating–substrate domination.

in the coating that supports a fraction of the load still play role in the system response, even at peak loads as high as 0.9 N.

The lower part of the unloading curve in Fig. 3(b) is of considerable interest. Since the nanoindenter utilized in this study is displacement controlled, any change in load applied to the indenter tip is registered. Therefore, the load-displacement response gives indication that during the last stages of unloading the sample is relaxing elastically and thus acts to push the indenter out (increasing the load at the apex), as if the coating has had popped up by propagation of a interfacial crack. To confirm this popping up of the coating, confocal microscopy of the indentations was performed. The results showed that when the nanoindentation curves presented this behavior, the indentation apex was located above the residual indentation depth, indicated by the load-displacement curve. For the nanoindentation of Fig. 3(b) a depth of approximately 800 nm was measured, indicating that after the indenter is removed, the coating surface within the annular crack is displaced above the residual position. Popping up of the coating did not occur beyond a certain maximum applied load (approximately 500 mN), presumably due to an almost complete through-thickness annular crack. Coated systems S1 and S2 share the same substrate and both have a chromium interlayer. Therefore, the evidence that uplifting of the coating had only occurred for coated system S2 suggests that the failure mechanism was decohesion within the coating, rather than debonding from the substrate. Moreover, Whitehead and Page[16] have proposed that interfacial crack propagation is more likely to take place in systems with a brittle substrate, where fracture is driven by the stored elastic energy across the interface. To certify that decohesion takes place only for coating system S2, the other systems were subjected to the maximum load available, 1 N, from the nanoindenter. As can be clearly observed from Figs. 3(a) and 3(c), the nanoindentation responses do not present evidence of coating delamination upon unloading.

The confirmation that the failure mechanism was decohesion within the coating was obtained by cross-sectioning the nanoindentations and inspecting them by SEM and TEM. Figure 6 shows an SEM micrograph of a cross-sectioned 400-mN nanoindentation. The area where the micrograph was taken can be precisely determined from the diameter of the annular crack and the orientation of the indenter tip. The presence of a brighter band in the coating is due to a higher tungsten concentration.[10]

The micrograph clearly establishes that the uplifting of the coating occurred not by interfacial fracture, but by crack propagation inside the coating. Furthermore, the cracks produced by tensile stresses, namely, the ones related to the indentation apex and the through thickness,

are also observed. It is noteworthy that the elastic strain energy stored within the coating due to bending is not enough, upon unloading, to debond the chromium interlayer from the steel substrate. Instead, as shown in Fig. 7(a), the energy is released by crack propagation in the carbon lamellae of the WC/C multilayers, where crack arrest occurs when the system reaches equilibrium. The crack propagates normal to the multilayers through carbon-enriched defects present in the coating, as seen in Fig. 7(b). These defects are created either by substrate surface irregularities or simply by the top morphology of the chromium columns.[10]

The explanation for crack propagation in the carbon lamellae (and ultimately leading to decohesion) of coated system S2, and not also of system S1, is related to their multilayers microstructure. From high-resolution TEM it could be learned that the multilayers have a different interlaminar structure. The lamellae thickness of systems S1 and T1 is approximately 6 nm for WC and approximately 2 nm for carbon, whereas for system S2 it is approximately 13 nm for WC and approximately 2.5 nm for carbon (cf. Fig. 1). Although the carbon lamellae have approximately the same thickness for the different coatings, the important feature for crack propagation is the existence of a sharp interface between the lamellae, which does not happen for systems S1 and T1, where the interface is rather diffuse. Moreover, the existence of an intermediate WC layer in the coating system S1 proves to be effective in supporting a fraction of the load and promoting the adhesion between the multilayers and the remaining coating.

The sequence of deformation events occurring during indentation is illustrated schematically in Fig. 8. Initially, only the coating deforms elastic-plastically (as is confirmed by the initial linear portion of the $P$-$\delta^2$ curve). Then, the substrate commences to experience a sufficiently high shear stress, which forces it to plastically yield. At the same time, the coating is bent to follow the substrate deformation and pile up, generating an increase on tensile stresses around the outer periphery of the contact zone. At a known, but slightly variable load (corresponding to the change in $P$-$\delta$ loading slope), the tensile stress reaches a maximum value, causing the coating to crack around the indentation periphery, resulting in an annular crack. Presumably at this critical load, the tensile stresses beneath the indenter apex are sufficiently high to start the crack propagation normal to the coating-substrate interface (this assumption was confirmed

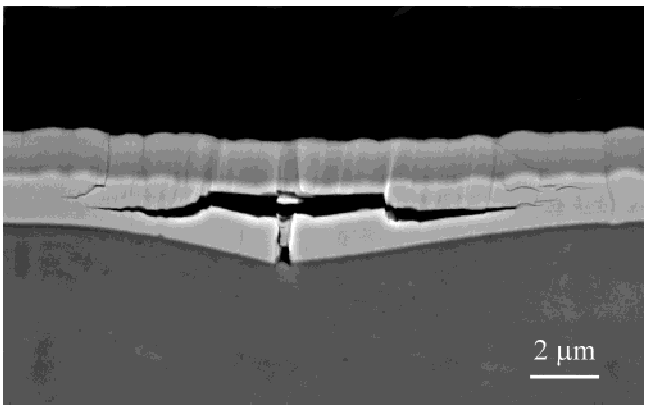


FIG. 6. SEM micrograph displaying a cross-section of a 400-mN nanoindentation on system S2. The coating contrast is related to dissimilarity in tungsten concentration, where brighter corresponds to a higher concentration. The right- and left-hand side cracks normal to the surface are from the annular crack formed around the indentation periphery, while the central crack was created by the indenter apex. The micrograph clearly establishes that the crack propagation occurred inside the coating.

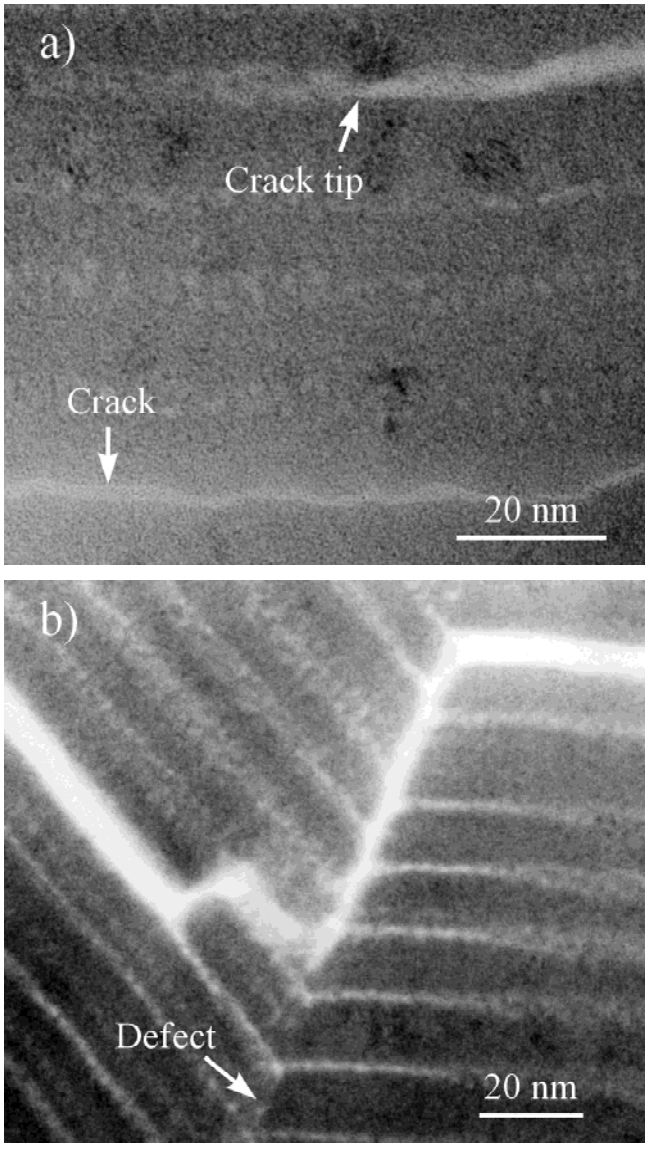


FIG. 7. Cross-sectional TEM images of the crack path. The images unequivocally confirm that the crack propagates in the carbon lamellae of the multilayers and glides through carbon-enriched defects, as indicated by the arrow.

experimentally by cross-sectioning a 200-mN nanoindentation). Increasing the load, the coating still plays some role in the deformation mechanism until the third regime in the $P$-$\delta^2$ curve is reached. Beyond that, the coating confined by the annular crack retains only a small portion of the membrane stresses and the substrate dominates the system response to deformation. When the load is released, the slope of the initially unloading curve is constant due to elastic recovery within the indentation. However, during the last stages of unloading very significant levels of elastic recovery occur followed by a sudden increase of the load at the indenter apex, corresponding to crack propagation inside the carbon lamellae parallel to the interface. The crack propagation is driven by the elastic strain energy stored within the coating free from the annular crack, i.e., the portion of the layer thickness beneath the through-thickness annular crack tip. The annular crack tip is always deflected outward from the indentation impression.

The cracks propagate until the system reaches equilibrium, which occurs further than the position of the annular crack. The nonobservance of coating uplifting for peak loads above approximately 500 mN is thought to be related to the elastic strain energy stored by bending of the small coating fraction beneath the annular crack tip. This energy is not enough to overcome the carbon cohesive energy and the energy necessary to push the coating volume (bounded by the annular crack) upwards.

### B. Mechanical properties

The load-displacement curve obtained from depth-sensing indentation enables one to get quantitative values for the hardness and modulus with accuracies better than 10%.[14] Nevertheless, previous work[19] has shown that for some materials the methodology can lead to significant overestimation of the hardness and modulus due to an underestimation of the true contact area, when a large amount of pile-up forms around the residual hardness impression. The underestimate of the contact area occurs because Eqs. (1) to (4) were derived from a purely elastic contact solution developed by Sneddon,[20] and therefore may not work well for elastic/plastic indentation. In the purely elastic contact solution, the material around the indenter always sink in, while for elastic/plastic indentation the material may either sink in or pile up. A method of characterizing materials for pile-up and the types where it is important have been developed in detail by Bolshakov *et al.*, using the finite element method.[21,22] A convenient, experimentally measurable parameter can be used to identify independently the expected indentation behavior of a given material. The parameter is the ratio of the final indentation depth to the displacement at peak load, $h_f/h_{max}$. When $h_f/h_{max} < 0.7$, very little pile-up is present, irrespectively of the work hardening behavior of the material. The observations leads to the conclusion that the hardness values obtained by the Oliver and Pharr method, i.e., using Eq. (1), are inaccurate only when the material piles up, which results in an underestimation of the real contact area. The reduced modulus, according to Eq. (2), is also overestimated when pile-up is important, $h_f/h_{max} > 0.7$, because the elastic solutions do not apply for a material with large plastic deformation. Curiously, finite element calculations show that even when pile-up is negligible, the reduced modulus is still overestimated by 2 to 9%. Taking into account the considerations drawn above on the influence of pile-up in quantifying the hardness and elastic modulus, all the indentations performed on the coated systems and substrates were checked for material pile-up. It was found that only the stainless steel substrate presented a large amount of pile-up around the hardness impression. Consequently, the hardness values measured for the coated systems might be considered accurate.

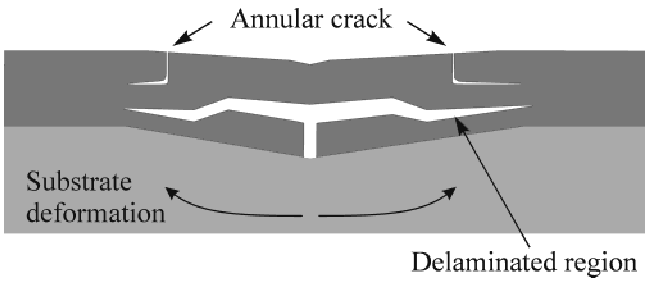


FIG. 8. Schematic diagram of the indentation-induced cracks which form on coated system S2.

The overestimation of the elastic modulus when measured by the Oliver and Pharr method was addressed by Hay *et al.*[23,24] It was established that a correction to Sneddon's solution for elastic contact by a rigid cone is needed to account for radial displacements. The correction factor ends on the Poisson's ratio of the indented material and the half angle of the indenter, $\phi$. For a Berkovich indenter, $\phi$ equals 70.32°. In the case of the present study, when the procedure for correction of the Sneddon's solution is applied, the hardness obtained by the Oliver and Pharr method, is underestimated by about 16.5%. The applicability of the correction factor to estimate the deviation on the effective Young's modulus is not straightforward as in the case of the hardness. However, for a material with $\nu = 0.25$, the correction reduces the effective modulus by about 7.4%. Thus, when the Oliver and Pharr method is applied to materials that do not exhibit pile-up, there is an explanation for the overestimation of the modulus observed in the finite element results.

Figure 9 shows the compositional hardness values measured as a function of peak load for as-deposited WC/C coatings onto steel substrates. In range of low

loads, the hardness values of the coated systems are similar. It validates the idea that the properties of the coatings can be measured at these depths of indentation. Thus, the hardness of WC/C can be estimated to be about 14 GPa, a value within the 10 to 40 GPa commonly reported for hard hydrogenated amorphous diamond-like coatings.[25–27] It is also interesting to analyze the hardness behavior with peak load. For coated system T1 the hardness is approximately constant. Therefore, the presence of nested cracks does not decrease the efficiency of the coating in supporting the load. Conversely, for systems S1 and S2 the appearance of annular cracks immediately decreases the ability of the coatings to support the load, and the properties of the stainless steel substrates start to come into sight. Further, the difference in hardness for systems S1 and S2 is associated with the structure of the coating itself, where for system S1 the presence of a WC interlayer promotes the load bearing capacity of the coating.

The effective Young's modulus values obtained as a function of peak load for the coated systems is shown in Fig. 10. Considering once more that the coating properties are probed at low loads, an effective modulus value of about 220 GPa can be obtained for the WC/C. For coated system T1, the modulus increases with the applied load approximating the values of the tool steel substrate, while for system S1 the value is almost constant. At low peak loads, system S2 has a higher effective modulus. This is thought to be due to dissimilarities in the WC/C multilayers, where the thicker WC lamellae could have

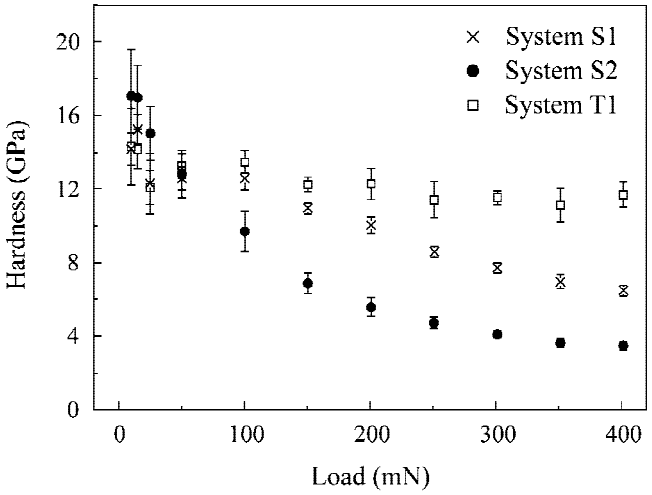


FIG. 9. Mean .compositional hardness values of the coated systems obtained from nanoindentation as a function of peak load.

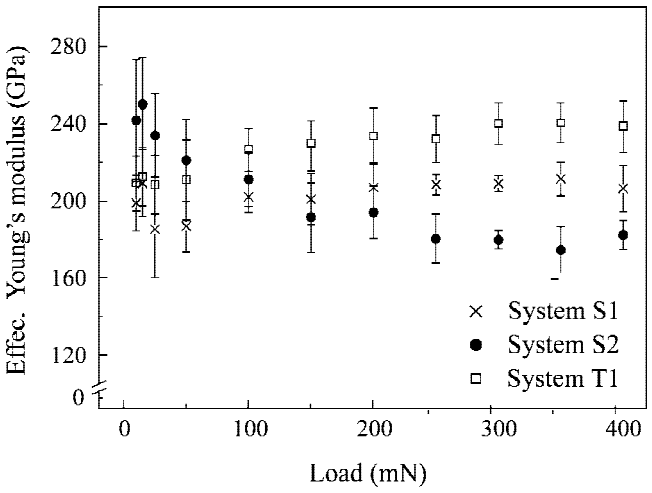


FIG. 10. Mean effective Young's modulus values of the coated systems obtained from nanoindentation as a function of peak load.

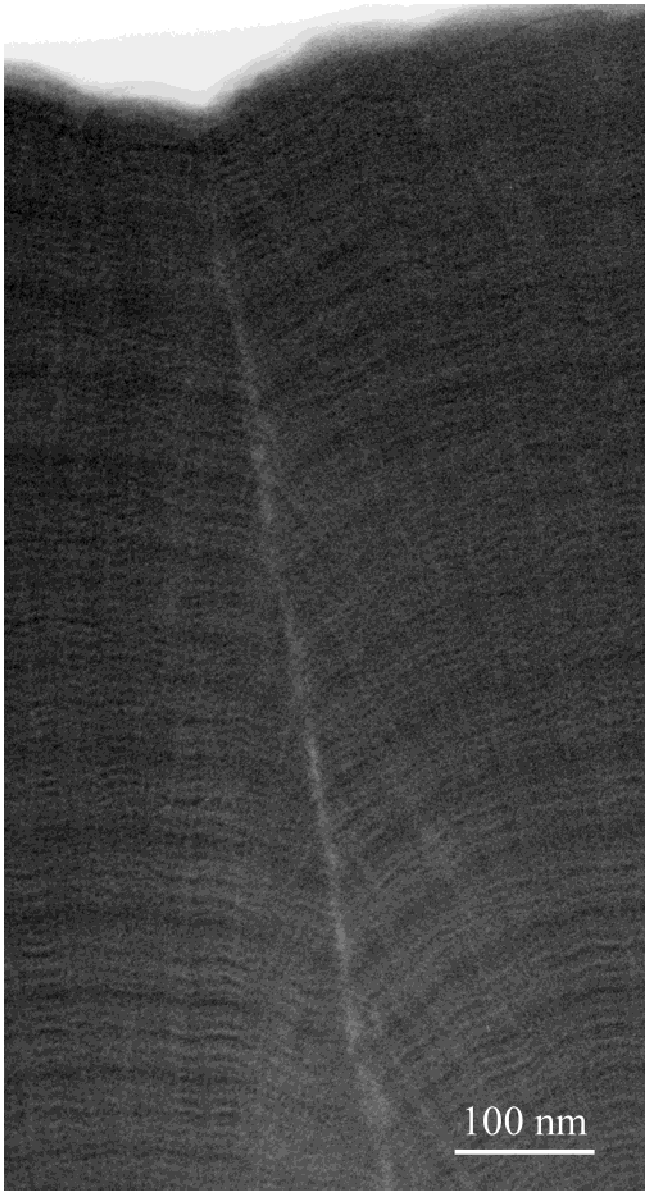


FIG. 11. Cross-sectional TEM image of the WC/C multilayers from the coated system S1 showing a surface groove created by a through-thickness defect.

increased the stiffness. To some extent, the scatter observed in the hardness and modulus values obtained at low peak loads is related to the place where the indentation is performed. When a nanoindentation is performed in a defect-free region the coating can deform under load to accommodate the indenter without failure due to the bending stresses generated. This is achieved by the shear that occurs in the elastic lamellae (carbon) allowing the brittle ones (WC) to slide over each other in the manner of a multileaf book when bent.[28] When nanoindenting on a surface groove, such as the one in Fig. 11, the defect in the coating inhibits sliding of the lamellae causing a localized increase in hardness. Logically, this effect is not observed at higher load. Consequently a small deviation in the hardness and modulus values is obtained.

## IV. CONCLUSIONS

In this work the nanoindentation response of structurally different WC/C multilayers, deposited onto stainless steel and tool steel substrates, has been investigated. The results are analyzed and discusses with support of planar and cross-sectional electron microscopy observations. The main conclusions are the following.

(1) Whenever the load-displacement curve shows a discrete change in slope, annular cracks around the indentation periphery are present.

(2) The deformation mechanism of coated systems depends on the substrate plastic properties. For stainless steel substrates, annular cracks are formed, while for tool steel, nested cracks are created.

(3) Combined analysis of $P$-$\delta$ and $P$-$\delta^2$ curves enables a more comprehensive characterization of the systems behavior.

(4) The nanoindentation response gives accurate information whether or not the coating has popped up during unloading.

(5) Cross-sectional electron microscopy of nanoindentations is a powerful method for investigation of the failure mechanisms of coated systems subjected to nanoindentations.

(6) The WC/C system responds to release of elastic strain energy by crack propagation in the carbon lamellae rather than by interfacial fracture.

(7) Care must be taken when designing a multilayers coating. The mechanical properties of each layer, thickness, and function must be analyzed thoroughly to optimize the system response.

## ACKNOWLEDGMENTS

The work described in this paper has been funded by the The Netherlands Organization for Applied Services Institute of Industrial Technology. The deposition of phase vapor deposition WC/C coatings on steel substrates by the Balzers Group is acknowledged. The authors thank Dr. W.P. Vellinga at the Faculty of Materials Technology and Mechanical Engineering from the University of Technology Eindhoven for the use of the nanoindenter and helpful discussion.

## REFERENCES

1. J. Güttler and J. Reschke, Surf. Coat. Technol. **60,** 531 (1993).
2. A. Matthews and S.S. Eskildesn, Diamond Relat. Mater. **3,** 902 (1994).
3. O. Wänstrand, M. Larsson, and P. Hedenqvist, Surf. Coat. Technol. **111,** 247 (1999).
4. G.M. Pharr, Mater. Sci. Eng. A **253,** 151 (1998).
5. T.F. Page and S.V. Hainsworth, Surf. Coat. Technol. **61,** 201 (1993).
6. T. Wright and T.F. Page, Surf. Coat. Technol. **54–55,** 557 (1992).
7. N.X. Randall, C.J. Schmutz, and J.M. Soro, Surf. Coat. Technol. **108–109,** 489 (1998).
8. S.V. Hainsworth, M.R. McGurk, and T.F. Page, Surf. Coat. Technol. **102,** 97 (1998).
9. M.R. McGurk, H.W. Chandler, P.C. Twigg, and T.F. Page, Surf. Coat. Technol. **68–69,** 576 (1994).
10. N.J.M. Carvalho and J.Th.M. De Hosson, Thin Solid Films **388,** 150 (2001).
11. K. Li, T.W. Wu, and J.C.M. Li, in *Thin Films: Stresses and Mechanical Properties VI,* edited by W.W. Gerberich, J-E. Sundgren, H. Gao, and S.P. Baker (Mater. Res. Soc. Proc. **436,** Pittsburgh, PA, 1997), p. 165.
12. M. Sakai, Acta Metal. Mater. **41,** 1751 (1993).
13. G.M. Pharr, W.C. Oliver, and F.R. Brotzen, J. Mater. Res. **7,** 613 (1992).
14. W.C. Oliver and G.M. Pharr, J. Mater. Res. **7,** 1564 (1992).
15. N.J.M. Carvalho, A.J. Huis in't Veld, W.P. Vellinga, and J.Th.M. De Hosson, in *Surface and Modification Technologies XII: Micro and Nanoindentation Studies of PVD TiN Coated Tool Steel,* edited by T.S. Sudarshan, K.A. Khor, M. Jeandin, and J. Stiglich (ASM, Materials Park, Ohio, 1998), p. 25.
16. A.J. Whitehead and T.F. Page, Thin Solid Films **220,** 277 (1992).
17. S.V. Hainsworth and T.F. Page, in *Thin Films: Stresses and Mechanical Properties VI,* edited by W.W. Gerberich, J-E. Sundgren, H. Gao, and S.P. Baker (Mater. Res. Soc. Symp. Proc. **436,** Pittsburgh, PA, 1997), p. 171.
18. M.R. McGurk and T.F. Page, J. Mater. Res. **14,** 2283 (1999).
19. T.Y. Tsui, W.C. Oliver, and G.M. Pharr, in *Thin Films: Stresses and Mechanical Properties VI,* edited by W.W. Gerberich, J-E. Sundgren, H. Gao, and S.P. Baker (Mater. Res. Soc. Symp. Proc. **436,** Pittsburgh, PA, 1997), p. 207.
20. I.N. Sneddon, Int. J. Eng. Sci. **3,** 47 (1965).
21. A. Bolshakov, W.C. Oliver, and G.M. Pharr, in *Thin Films: Stresses and Mechanical Properties VI,* edited by W.W. Gerberich, J-E. Sundgren, H. Gao, and S.P. Baker (Mater. Res. Soc. Symp. Proc. **436,** Pittsburgh, PA, 1997), p. 141.
22. A. Bolshakov and G.M. Pharr, J. Mater. Res. **13,** 1049 (1998).
23. J.C. Hay and G.M. Pharr, in *Fundamentals of Nanoindentation and Nanotribology,* edited by N.R. Moody, W.W. Gerberich, N. Burnham, and S.P. Baker (Mater. Res. Soc. Symp. Proc. **522,** Warrendale, PA, 1998), p. 39.
24. J.C. Hay, A. Bolshakov, and G.M. Pharr, J. Mater. Res. **14,** 2296 (1999).
25. J. Franks, K. Enke, and A. Richardt, Metals and Materials **11,** 695 (1990).
26. M. Ham and A. Lou, J. Vac. Sci. Technol. **A8,** 2143 (1990).
27. A. Raveh, L. Martinu, H.M. Hawthorne, and M.R. Wertheimer, Surf. Coat. Technol. **58,** 45 (1993).
28. A. Matthews, A. Leyland, K. Holmberg, and H. Ronkainen, Surf. Coat. Technol. **100–101,** 1 (1998).